Journal of Alloys and Compounds 509 (2011) 8350–8355

Contents lists available at ScienceDirect

Journal of Alloys and Compounds

journal homepage: www.elsevier.com/locate/jallcom

Influence of thermally induced structural transformations on hardness in $Fe_{89.8}Ni_{1.5}Si_{5.2}B_3C_{0.5}$ amorphous alloy

D.M. Minić[a,*], V. Blagojević[a], D.G. Minić[b], A. Gavrilović[c], L. Rafailović[c]

[a] Faculty of Physical Chemistry, University of Belgrade, Belgrade, Serbia
[b] Kontrola LLC, Austin, TX, USA
[c] CEST, Centre of Electrochemical Surface Technology, Wiener Neustadt, Austria

ARTICLE INFO

Article history:
Received 13 November 2010
Received in revised form 2 March 2011
Accepted 3 March 2011
Available online 10 March 2011

Keywords:
Metallic glasses
Nanostructured materials
Composite materials
X-ray diffraction
Microhardness

ABSTRACT

Effect of heat treatment on mechanical behavior of $Fe_{89.8}Ni_{1.5}Si_{5.2}B_3C_{0.5}$ amorphous alloy was investigated by measuring microhardness. It was shown that the as-prepared amorphous alloy has an unexpectedly high microhardness. This can be attributed not only to boron dispersed in the alloy, but also to the structure which exhibits aspects of a nanocomposite of nanoparticles dispersed in an amorphous matrix. As the alloy crystallizes at temperatures above 540 °C, microhardness decreases continuously as a function of heating temperature. This is attributed to separation of boron out of the amorphous matrix into nanocrystals of Fe_2B phase. Further decrease in microhardness is attributed to crystallite growth with the accompanying change in the dominant nature of the interfaces from amorphous/crystal to crystal/crystal, and creation of a porous structure. When the crystallization is complete, the alloy exhibits microhardness close to that of a hypothetical mixture of α-Fe and Fe_2B phases of the same composition.

1. Introduction

Iron-based amorphous alloys have been a subject of considerable scientific interest, because of their soft ferromagnetic properties (saturation magnetization, high permeability, low coercivity and loss), high corrosion resistance and good mechanical properties [1,2]. This makes them suitable for use in a variety of applications [3–6], but their application as structural materials has been limited by high cooling rates required to avoid crystallization and their tendency to oxidize. Magnetic properties of amorphous Fe-based alloys could deteriorate after crystallization, or, if nanocrystalline phases are formed, they may be improved [7–10], producing functional materials with targeted properties. Commercial soft magnetic nanocrystalline materials, exhibiting superior soft magnetic and mechanical properties, have recently been successfully obtained by crystallization of amorphous precursors. These materials are characterized by a microstructure of nanocrystals dispersed in an amorphous matrix. Recent theoretical studies of iron-based binary systems predict existence of short-range ordering in iron-based amorphous alloys. Theoretical investigation of nanoscale phase separation in small $Fe_{80}B_{20}$ and $Fe_{83}B_{17}$ clusters [11] predicts formation of Fe-pure regions, Fe-rich regions (which contain around 9% B) and B-rich regions. Additionally, Lass et al. [12] predicted presence of short-range chemical ordering in Fe-based binary systems and found that predicted coordination numbers for Fe–P and Fe–B alloys were in good agreement with experimental results.

Thermal stability of these alloys and its correlation with electrical and magnetic properties have been a focus of some interest [13–16], but there has not been much discussion of the correlation of thermal stability with mechanical properties. Mechanical properties of iron-based amorphous alloys [17,18] have been studied in some detail lately, but there have been very few studies that discuss the correlation of microstructure or phase composition of these alloys with their mechanical properties. Recent study of rapidly quenched iron alloy with 6.5% Si [19] found that rapid quenching resulted in smaller grain size in the alloy samples than conventional casting and decreased microhardness. The authors attributed this to suppression of first-order phase transformation in crystalline iron. Recent studies of hardness of iron-based alloy powders [20] revealed that, when going from crystalline towards amorphous sample, hardness reaches a maximum when the sample is composed of a mix of crystalline nanoparticles and amorphous phase, and then begins to decrease as the amorphous content of the sample is further increased. The authors attribute this effect to dense packing of crystalline nanoparticles, which have substantial hardness, because of relative lack of defects, in an amorphous matrix. Amorphous/crystal interface has lower interfacial energy than crystal/crystal interface [21] and this structure suppresses propagation of shear bands and cracks along these interfaces. Finally,

* Corresponding author. Tel.: +381 11 3336 689; fax: +381 11 2187 133.
E-mail addresses: dminic@ffh.bg.ac.rs, drminic@gmail.com (D.M. Minić).

0925-8388/$ – see front matter © 2011 Elsevier B.V. All rights reserved.
doi:10.1016/j.jallcom.2011.03.011

the dispersion of the nanoparticles probably suppresses the deformation of the amorphous phase through shear sliding. Because of these mechanisms, the nanocomposites of crystalline nanoparticles and amorphous phase should have higher microhardness than either pure crystalline or pure amorphous phase. A recent study investigated the relationship between thermophysical and mechanical properties of amorphous alloys [22] in order to develop a generalized picture of shear band propagation. Investigation of microhardness in boronizing layers of Fe-powder compacts [23] showed that, when iron particles are doped with boron through sintering of iron powders at temperatures above 1000 °C, the surface structure of the particles exhibits three distinct areas, going from the surface down into the layer: surface boride zone is followed by a transition zone of diminishing boron content and then, finally, the iron matrix without any boron. Microhardness of the surface boride layer is 1487–2066 HV, depending on its thickness—as the thickness of the layer increases, so does microhardness. Average microhardness of the transition layer is 855 HV.

Our previous study of different aspects of structural transformations of $Fe_{89.8}Ni_{1.5}Si_{5.2}B_3C_{0.5}$ amorphous alloy focused on thermal stability [24] and the correlation of structural transformations with electrical and magnetic properties [25,26]. The focus of this research has been the relationship between structural transformations of the alloy and its mechanical properties, in particular the microhardness. In particular, we discussed in detail the influence of changes in microstructure, as well as phase composition of the alloy, over 25–850 °C temperature range.

2. Experimental

$Fe_{89.8}Ni_{1.5}Si_{5.2}B_3C_{0.5}$ amorphous alloy samples were prepared in form of ribbon, 2 cm wide and 35 μm thick, using the standard procedure of rapid quenching of a melt on a rotating disc (melt spinning method). The ribbon samples were thermally treated, under vacuum in quartz ampoules, at different temperatures (up to 850 °C) for 1 h and then left to cool down to room temperature, before investigating their properties.

X-ray diffraction spectra were acquired on X-Pert powder diffractometer (PANalytical, Netherlands) using CuKα radiation in Bragg-Bentano geometry at 40 kV and 30 mA. This instrument is equipped with a secondary graphite monochromator, automatic divergence slits and a scintillation counter. The collection of data was performed with 0.05° step in diffraction angle and the collection time of 30 s per step. Analysis of XRD spectra was performed using Rietveld refinement method and single peak refinement approach, with TOPAS v.3.0 general profile and structure analysis software [27]. Dislocation density was obtained from the Rietveld analysis, while microstrain was calculated using Williamson-Hall method [28], using the XRD data.

Vickers microhardness tests were performed using MHT-10 (Anton Paar, Austria) microhardness tester, with loads of 0.4 N and loading time of 10 s. Up to seven measurements were performed on each individual sample and used to determine the average value of microhardness for each sample. Surface-to-volume ratio of the crystallites was estimated using the average crystal size of individual crystal phases, by approximating that all the crystallites were spherical in shape. The calculated surface-to-volume ratio represents an estimate of total surface-to-volume ratio for crystalline phases in alloy samples.

SEM images were obtained using XL 30 ESEM-FEG (Environmental Scanning Microscope with Field Emission Gun, by FEI, Netherlands), with 20 kV acceleration voltage, at magnifications of 3500× and 20,000×.

3. Results

X-ray diffraction (XRD) spectra (Fig. 1) of $Fe_{89.8}Ni_{1.5}Si_{5.2}B_3C_{0.5}$ alloy at room temperature showed a relatively strong broad peak around 44° and another, much smaller and also broad peak around 80°. XRD spectra of the alloy after thermal treatment at different temperatures (Fig. 2) showed that the alloy begun to crystallize when the temperature reached around 480 °C, and around 540 °C sharp peaks of α-Fe(Si) crystalline phase were already present in the spectra. This phase was a result of high tendency of Si to dissolve in Fe. Before crystallization, around 300 °C, the broad peaks present at room temperature decreased in intensity, giving way to a broad signal that could be attributed to the amorphous part of

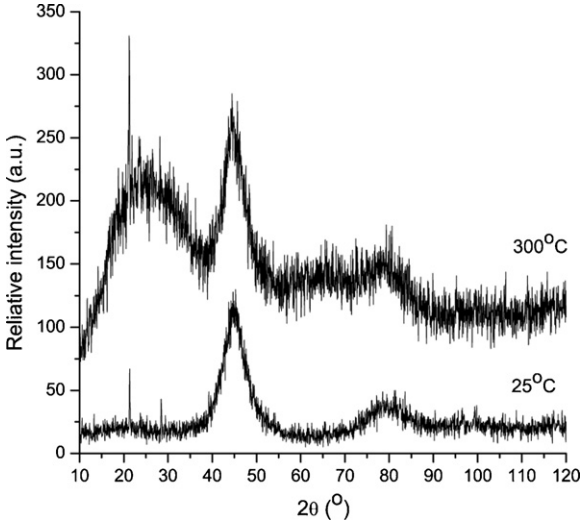

Fig. 1. XRD spectra of $Fe_{89.8}Ni_{1.5}Si_{5.2}B_3C_{0.5}$ amorphous alloy on preparation and before the onset of crystallization.

the sample. A meta-stable minor phase $Fe_{15}B_2Si_3$ was present only at 540 °C, and disappears at higher temperatures. XRD spectra at 570 °C and above showed formation of Fe_2B crystalline phase. As the alloy samples were treated at higher temperatures, the degree of crystallinity of the alloy increased quickly, until the heating temperature of 650 °C, and slowly after that. Phase composition of the alloy (Table 1) shows that, at temperatures above 500 °C, α-Fe(Si) was the dominant crystalline phase, reaching about 77% of the total mass of the sample after thermal treatment at 850 °C. Fe_2B began to crystallize at 570 °C and accounted for about 20% of the mass of the sample at 850 °C. Meta-stable phase $Fe_{15}B_2Si_3$ was present only after treatment at 540 °C, at around 3 mass%. Amorphous phase content was determined as the difference of the sum of the contents of crystalline phases to 100 mass%. When $Fe_{89.8}Ni_{1.5}Si_{5.2}B_3C_{0.5}$ alloy was thermally treated at 850 °C for 7 h, the final composition of the alloy was 61% α-Fe(Si) and 39% Fe_2B phase. In molar percentages, this translates as 77.5 mol% α-Fe(Si) and 22.5 mol% Fe_2B.

SEM images (Fig. 3) of $Fe_{89.8}Ni_{1.5}Si_{5.2}B_3C_{0.5}$ alloy surface showed homogenous amorphous surface before thermal treatment (Fig. 3a)

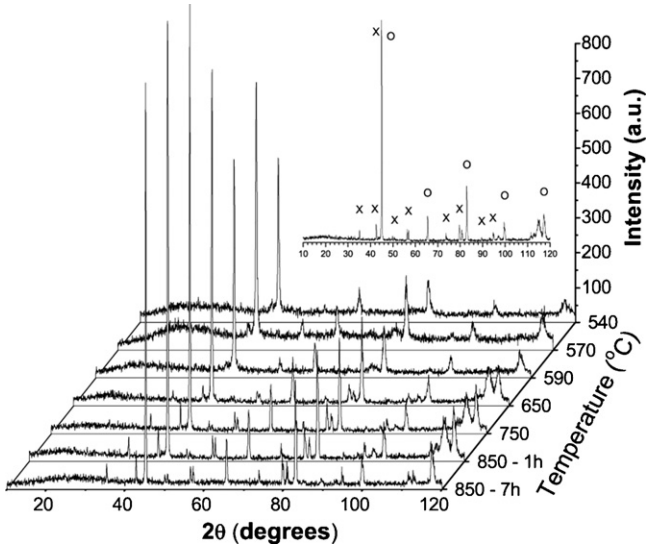

Fig. 2. XRD spectra of $Fe_{89.8}Ni_{1.5}Si_{5.2}B_3C_{0.5}$ amorphous alloy after thermal treatment at different temperatures, after the onset of crystallization (inset, o—a-Fe(Si) and x—Fe_2B).

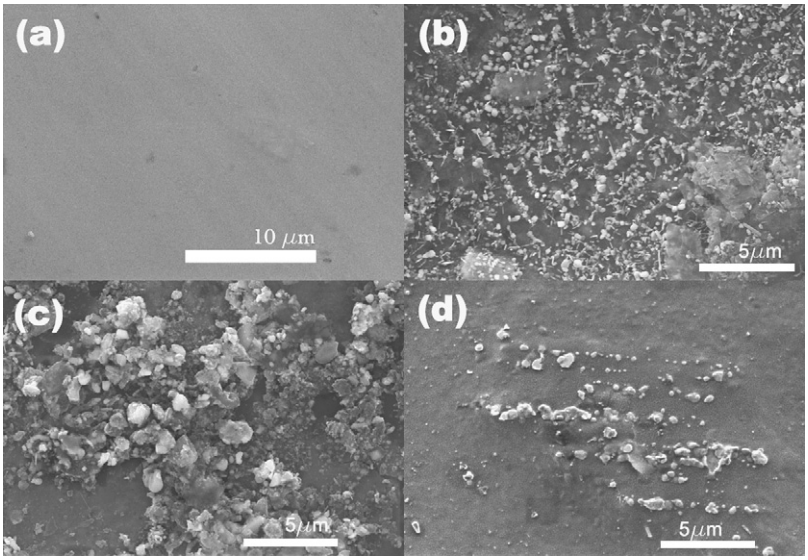

Fig. 3. SEM images of $Fe_{89.8}Ni_{1.5}Si_{5.2}B_3C_{0.5}$ alloy before thermal treatment (a) and after (b: 650 °C, c: 750 °C, and d: 850 °C).

and granulated surface due to gradual crystallization after the thermal treatment (Fig. 3b–d). The crystallization occurred, initially, through growth of a large number of smaller crystals (Fig. 3b) up to 650 °C, followed by the growth of larger crystals at 750 °C (Fig. 3c). After the alloy was thermally treated at 850 °C (Fig. 3d), the formation of a much more homogenous surface, compared to the sample thermally treated at 750 °C, was observed.

Average crystal size at different temperatures was determined using Rietveld analysis of XRD spectra.

The dependence of crystal size with respect to temperature (Fig. 4) showed that the crystal size of Fe_2B decreased initially, going from 570 to 590 °C, and then increased continuously above 590 °C. α-Fe(Si) crystalline phase showed rapid growth in two temperature regions: 590–650 °C and above 750 °C. In the regions below 590 °C and 650–750 °C, α-Fe(Si) phase crystals grew very slowly—29–32 nm and 57–60 nm, in the respective temperature regions. When the sample was thermally treated at 850 °C for 7 h, the average crystalline size of α-Fe(Si) increased from 101 to 123 nm, while that of Fe_2B increased from 119 to 178 nm.

As part of detail study of the microstructure of the alloy samples, we calculated dislocation density and microstrain using the XRD data. Dislocation density (Table 1) in Fe_2B showed sharp increase going from 570 °C to 590 °C, followed by steep decline above this temperature. In α-Fe(Si) phase, dislocation density showed a steady decrease through the entire heating process, relatively slow in the initial temperature region, below 590 °C, and more pronounced at 650 °C. The decrease slowed down again above 650 °C. After thermal treatment at 850 °C, the dislocation density in Fe_2B became lower than that in α-Fe(Si) nanocrystals. After thermal treatment at 850 °C for 7 h, the dislocation density declined even further, again, more in Fe_2B than in α-Fe(Si) nanocrystals.

Microstrain in the alloy (Fig. 4) decreased after the alloy was thermally treated at temperatures below 650 °C and after thermal treatment at 850 °C and increased going from 650 °C to 750 °C. After thermal treatment at 850 °C for 7 h, microstrain declined even further, when compared with samples heated for 1 h, to 1.8%.

Microhardness (Fig. 5) of as-prepared alloy was 926 HV, and declined to 884 HV, after the sample was thermally treated at 300 °C and to 846 HV after treatment at 540 °C. After further thermal treatment at temperatures above 540 °C, it decreased to a minimum of 612 HV after thermal treatment at 850 °C. After the sample was thermally treated for 7 h at 850 °C, microhardness was determined to be 689 HV.

Table 1
Phase composition and dislocation density of individual crystal phases in alloy samples thermally treated at different temperatures.

Temperature (°C)	α-Fe(Si)	Fe_2B	$Fe_{15}B_2Si_3$	Amorphous
Phase composition (mass%)				
540	38	–	2	60
570	46	7	–	43
590	52	12	–	36
650	73	17	–	10
750	72	19	–	9
850	77	20	–	3
Dislocation density (10^{14} m^{-2})				
540	35.7	–		
570	33.3	117		
590	29.3	208		
650	9.23	23.1		
750	8.33	7.32		
850	2.94	2.12		

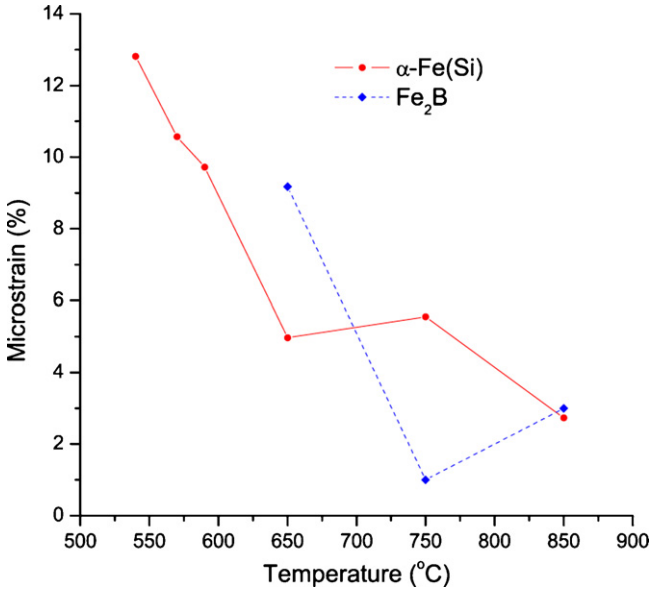

Fig. 4. Change in microstrain of $Fe_{89.8}Ni_{1.5}Si_{5.2}B_3C_{0.5}$ amorphous alloy on thermal treatment.

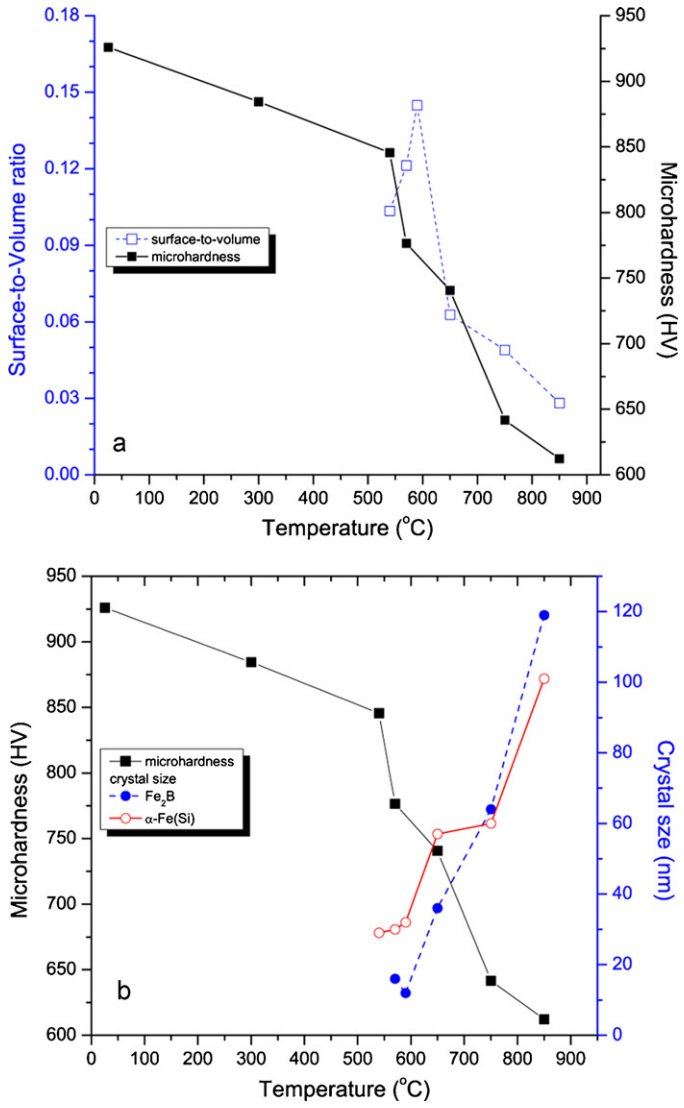

Fig. 5. Change in microhardness of $Fe_{89.8}Ni_{1.5}Si_{5.2}B_3C_{0.5}$ amorphous alloy on thermal treatment with (a) surface-to-volume ratio and (b) average crystal size.

4. Discussion

4.1. Thermally induced structural transformations

X-ray diffraction spectrum (Fig. 1) of the alloy at room temperature showed two broad peaks: around 44° and around 80°. These positions correspond to the positions of most intense peaks of the two crystalline phases: α-Fe(Si) and Fe_2B, respectively [ICDD PDF 00-036-4899 and 00-036-1332]. This indicates that the as-prepared alloy was not completely amorphous and had some crystalline character, probably in form of short-range crystalline ordering, with characteristics of the two crystalline phases that appear after the samples are heated. This is in agreement with theoretical investigations of iron–boron systems [11], which predicts formation of Fe-pure regions in parallel with Fe-rich regions (which contain around 9% B, compared to 8.88% B in Fe_2B) and B-rich regions. Since our alloy contained much smaller Fe-to-B ratio than these clusters (around 30:1, compared to 4:1 and 5:1, respectively), it is possible that the two peaks belonging to α-Fe(Si) and Fe_2B correspond to Fe-pure regions and Fe-rich regions described above. The overall alloy structure at room temperature could be described as a very fine nanocomposite of small nanoclusters dispersed in the amorphous matrix. After the alloy was thermally treated to 300 °C, another broad peak appeared, centered around 25°, which could be attributed to the amorphous content of the sample. Its absence at room temperature indicates that it appears as a result of disordering of the as-prepared alloy structure due to thermal treatment. It also gives us an indication that the as-prepared alloy structure seems to be much more organized than one would expect from a completely amorphous sample. The XRD spectra of the samples thermally treated at 540 °C and above showed crystallization of two stable crystalline phases (α-Fe(Si) and Fe_2B) and a meta-stable $Fe_{15}B_2Si_3$ phase, which only appeared at 540 °C, suggesting that the meta-stable phase was an intermediate phase in the initial stage of crystallization of Fe_2B. Phase composition (Table 1) showed that most of the crystallization occurred below 650 °C as the percentage of amorphous content dropped from 60 mass% to 10 mass%, going from 540 to 650 °C, with α-Fe(Si) being the dominant crystalline phase. After that α-Fe(Si) phase content decreased slightly at 750 °C and increased again at 850 °C. This behavior between 650 °C and 850 °C was reflected in the amorphous content of the sample, which, after the sharp decline, dropped from 10% to 9% going from 650 °C to 750 °C and then to 3% going to 850 °C. When the sample was thermally treated for 7 h at 850 °C, the phase mass content was 61% α-Fe(Si) and 39% Fe_2B, indicating that the crystallization was complete at this point, since amorphous phase was completely gone and mass percentage of Fe_2B corresponded to the boron content of the as-prepared alloy.

SEM images (Fig. 3) showed smooth surface in amorphous sample at room temperature and then the presence of smaller and lager crystals after thermal treatment at 650 °C and 750 °C, respectively. After thermal treatment at 850 °C the sample showed much smoother surface than at 750 °C, indicating that the surface had reformed and the individual crystals had probably reoriented and merged together.

4.2. Evolution of microstructure

In order to conduct a more detailed analysis of the microstructure, we determined average crystal size, dislocation density and microstrain for each crystal phase. These parameters could offer further insight into causes of structural transformations and their influence on the mechanical properties of alloy samples. The dependence of average crystal size (Fig. 5b) of the dominant phase on the heating temperature showed two major increases—below 650 °C and above 750 °C, mirroring the phase composition change (Table 1). Nucleation was the dominant process below 600 °C, as indicated by relatively stable crystal size and high dislocation density (Table 1). After treatment at 650 °C, crystal growth was accelerated—the crystal size increased rapidly and dislocation density and microstrain decreased, indicating that larger crystals were formed. After that, the crystalline size remained almost stable, mass percentage of α-Fe(Si) crystalline phase declined, dislocation density showed a slight decrease and microstrain increased. These indicate that a nanocomposite of nanocrystals in an amorphous matrix had been formed, with amorphous matrix occupying the space between nanocrystals. The nanocrystals grew until the system reached a point where the difference in interfacial energy of existing amorphous/crystal interface and crystal/crystal interface forced the crystalline phase to reorganize through recrystallization in order to accommodate further growth.

The in-depth analysis of the XRD spectra supported this, indicating that significant change in aspect ratio of α-Fe(Si) crystallites occurred in this temperature region, manifesting itself as a change in the ratio of full-widths at half-maxima of peaks corresponding to (1 0 0) and (2 1 1) crystalline planes. Judging by this, the crystallites formed at 650 °C exhibited more symmetrical shape than

those formed at 750 °C. The asymmetrical shape of the larger crystallites was a result of rapid growth. The average crystal size almost doubled going from 750 °C to 850 °C, as the crystal shape changed to a more symmetrical one and the sample surface becomes much smoother. Dislocation density and microstrain declined, indicating that α-Fe(Si) crystals had formed with better defined crystal facets, which were accommodated by the increased size of the crystals. Mass percentage of α-Fe(Si) in the sample increased from 72% to 77%, while amorphous phase content declined from 9% to 3%.

Fe_2B started to crystallize around 570 °C, with average crystal size of 16 nm, when it accounted for around 7% of the total mass. When the sample was heated at 590 °C, the mass percentage of Fe_2B increased to 12%, while average crystal size decreased to 12 nm. Dislocation density in Fe_2B increased (Table 1), going from 570 to 590 °C, which reflected the decrease in average crystal size (Fig. 5b). Fe_2B crystals could be initially formed as one of the products of decomposition of the meta-stable $Fe_{15}Si_3B_2$ phase. The initial nucleation was followed by very rapid crystal growth above 590 °C, as the average crystal size increased from 12 to 36 nm, going from 590 °C to 650 °C. The phase content percentage increased from 12% to 17%, and dislocation density declined rapidly. SEM image of sample heated at 650 °C (Fig. 3b) showed a large number of small nanoparticles on the surface of the alloy, indicating that Fe_2B phase probably separated as individual crystals from the alloy at this point. The crystal size continued to increase (64 nm at 750 °C and 119 nm at 850 °C), while the mass percentage of the Fe_2B phase remained relatively stable (19% at 750 °C and 20% at 850 °C). This indicated that the rapid growth of Fe_2B, up to this point, was mostly at the expense of the amorphous phase, while the growth above 650 °C probably happened through merging of smaller crystals or their dissolution and incorporation into larger crystals. This is supported by continued sharp decline in dislocation density. SEM images of samples heated at 750 °C and 850 °C (Fig. 3c and d) show a contrasting image: at 750 °C the surface had a large number of nanoparticles on the surface, consistent with the growth of nanocrystals going from 650 °C to 750 °C; at 850 °C the surface was much smoother and the nanoparticles visible seemed to be merged with the surface of the alloy. This indicates that, as the heating temperature was increased and Fe_2B phase separated out from the alloy, the structure of the alloy changed to accommodate for the incorporation of these crystals back into the alloy. This is supported by the changes in the microstrain of the alloy ribbon (Fig. 4), which showed a decrease at 850 °C, after an increase at 750 °C. After the sample was thermally treated for 7 h at 850 °C, boron completely separated into Fe_2B phase.

4.3. Influence of structural changes on mechanical properties

The influence of microstructural changes studied here on mechanical properties of the alloy was investigated by measuring microhardness of alloy samples, thermally treated at different temperatures. Microhardness (Fig. 5) of the as-prepared alloy at room temperature was 924 HV, which is unexpectedly high. After the alloy was thermally treated at 300 °C for an hour, it exhibited a lower degree of ordering and this was accompanied by a decrease in microhardness, to 884 HV. At the early stage of crystallization of the alloy, at 540 °C, the microhardness declined further, to 846 HV. This value corresponds well to microhardness of intermediate layer found in crystalline boron doped iron powders [23]. The increased microhardness of as-prepared alloy can be attributed to the fact that the alloy exhibits some degree of ordering, similar to nanocomposites of nanoparticles dispersed in an amorphous matrix. Nanocomposites of nanocrystals dispersed in an amorphous matrix have been shown to perform better in microhardness tests than either pure crystalline or amorphous phases of the same material. Therefore, since the as-prepared alloy at room temperature exhibited a higher degree of ordering than after thermal treatment and before the onset of crystallization, it is expected that this ordering resulted in higher microhardness.

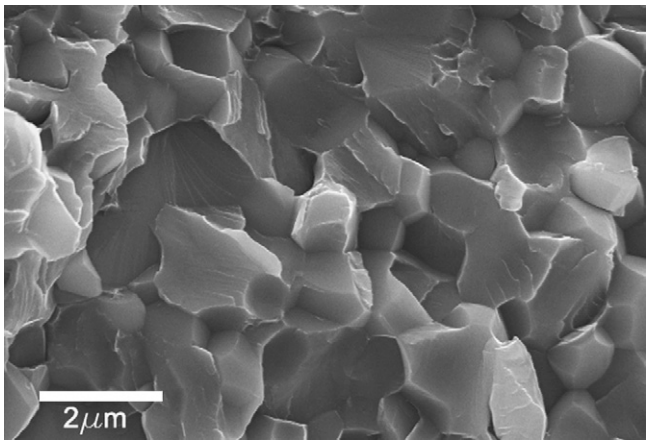

Fig. 6. SEM of the cross-section of alloy sample treated at 850 °C for 7 h.

At higher temperatures, above 540 °C, microhardness showed a sharp decline, which is consistent with the loss of boron from the amorphous matrix due to crystallization. Further decline in microhardness (Fig. 5) was caused by the growth of the crystallites, through two contributing factors: increase of crystal/crystal interfaces, as opposed to amorphous/crystal, and creation of more porous structure in the alloy samples (Fig. 6). Crystal/crystal interfaces are more susceptible to propagation of shear bands and cracks along these interfaces than amorphous/crystal, resulting in diminished microhardness. The alloy sample which was thermally treated for 1 h at 850 °C exhibited the lowest value of microhardness at 612 HV. Prolonged thermal treatment at 850 °C (7 h), led to an increase in microhardness to 689 HV. Therefore, microhardness increased in spite of very porous structure of the alloy sample, as can be seen on SEM of its cross-section (Fig. 6). This could be attributed to several factors: higher percentage of Fe_2B phase in the latter sample (39 mass% as compared to 20 mass%) and loss of crystal/crystal interfaces through sintering of the crystalline grains. In consequence, this very porous structure of the sample treated at 850 °C for 7 h, exhibited much better mechanical properties when compared to the sample treated at the same temperature for 1 h.

In order to compare the properties of our alloy sample treated at 850 °C for 7 h, with the properties of the respective constituents in their respective molar fractions, we estimated hardness of such hypothetical mixture, based on the literature data for the individual component phases. α-Fe phase on its own has a microhardness of about 250 HV [29] and the iron-boride phase has much higher microhardness of up to 2066 HV. When the alloy was thermally treated at 850 °C for 7 h, the crystallization was complete and relative molar ratio of the two phases was 3.44:1 in favor of α-Fe(Si). If we use the microhardness of pure α-Fe (since the amount of Si is relatively small and its addition only increases hardness of α-Fe), the projected lower limit of average value for 3.44:1 mixture of α-Fe(Si) and Fe_2B would be around 660 HV, which is very close to 689 HV, microhardness of alloy sample treated at 850 °C for 7 h. This indicates that, after our alloy fully crystallized, Fe_2B crystallites are dispersed in α-Fe(Si) nanocrystalline matrix in a relatively homogenous manner, so that the alloy exhibited, at the macroscopic level, mechanical properties that could be attributed to a hypothetical mixture of these two phases.

5. Conclusions

Here we present the examination of structural transformations of $Fe_{89.8}Ni_{1.5}Si_{5.2}B_3C_{0.5}$ amorphous alloy induced by thermal treatment and the effect of these transformations on its mechanical properties (microhardness in particular). Microhardness of as-prepared amorphous alloy was unexpectedly high, 924 HV, because the alloy exhibited a degree of ordering which could correspond to a structure involving nanoclusters dispersed in an amorphous matrix containing boron, which increased microhardness of the alloy. The crystallization process was characterized by gradual separation of two crystalline phases: α-Fe(Si) and Fe_2B, and was completed when the sample is thermally treated at 850 °C for 7 h, with distribution of mass being 61% of α-Fe(Si) and 39% of Fe_2B. During the crystallization process, we observed a continuous decline in the microhardness, starting from 570 °C, corresponding to gradual separation of boron out of the amorphous alloy into the separate Fe_2B crystalline phase and formation of nanocrystalline granulated structure. This led us to conclude that the presence of boron was the major contributor to the microhardness of the amorphous alloy. Further growth of Fe_2B nanocrystals at higher temperatures led to additional decline in microhardness, because the dominant type of interface changed from amorphous/crystal to crystal/crystal. Microhardness of fully crystallized mixture of α-Fe(Si) and Fe_2B was close to a calculated average value of microhardness for the mixture of the same molar ratios of α-Fe and Fe_2B phases.

Acknowledgements

The investigation was partially supported by the Ministry of Science and Environmental Protection of Serbia, under the following Project and 172015. The work at CEST was supported within the COMET program by the Austrian Research Promotion Agency (Österreichische Forschungförderungsgesellschaft, FFG) and the government of Lower Austria.

References

[1] K. Biswas, S. Ram, L. Schultz, J. Eckert, J. Alloys Compd. 397 (2005) 104.
[2] A.L. Greer, Curr. Opin. Solid State Mater. 2 (1997) 412.
[3] J. Long, M. McHenry, D.P. Urciuoli, V. Keylin, J. Huth, T.E. Salem, J. Appl. Phys. 103 (2008) 07E705.
[4] L.K. Varga, J. Magn. Magn. Mater. 316 (2007) 442.
[5] L.J. Wang, J.Q. Li, S.H. Li, G.Q. Zhang, S.L. Huang, J. Appl. Mech. Mater. 48–49 (2011) 246.
[6] N. Nishiyama, K. Takenaka, N. Togashi, N. Miura, N. Saidoh, A. Inoue, Intermetallics 18 (2010) 1983.
[7] D.M. Minić, A.M. Maričić, R.Z. Dimitrijević, M.M. Ristić, J. Alloys Compd. 430 (2007) 241.
[8] H.F. Li, R.V. Ramanujan, Mater. Sci. Eng. A 375 (377) (2004) 1087–1091.
[9] J. Bednarick, R. Nicula, M. Stir, E. Bukel, J. Magn. Magn. Mater. 316 (2007) e823.
[10] M.E. McHenry, M.A. Willard, D.E. Laughlin, Prog. Mater. Sci. 44 (1999) 291.
[11] M. Aykol, A.O. Mekhrabov, M.V. Akdeniz, Acta Mater. 57 (2009) 171.
[12] E.A. Lass, A. Zhu, G.J. Shiflet, S.J. Poon, Acta Mater. 58 (2010) 5460.
[13] E. Thirumal, D. Prabhu, K. Chattopadhyay, V. Ravichandran, Phys. Status Solidi A 207 (2010) 2505.
[14] S. Bhattacharya, E.A. Lass, S.J. Poon, G.J. Shiflet, J. Alloys Compd. 488 (2009) 79.
[15] X.F. Miao, Y.G. Wang, M. Guo, J. Alloys Compd. 509 (2011) 2789.
[16] T. Saito, J. Alloys Compd. 505 (2010) 23.
[17] H. Jian, W. Luo, S. Tao, M. Yan, J. Alloys Compd. 505 (2010) 315.
[18] J.J. Lewandowski, X.J. Gu, A.S. Nouri, S.J. Poon, G.J. Shiflet, Appl. Phys. Lett. 92 (2008) 091918.
[19] Y.F. Liang, J.P. Lin, F. Ye, Y.J. Li, Y.L. Wang, G.L. Chen, J. Alloys Compd. 504S (2010) S476.
[20] E. Salahinejad, R. Amini, E. Askari Bajestani, M.J. Hadianfard, J. Alloys Compd. 497 (2010) 369.
[21] S. Stankov, M. Miglierini, A.I. Chumakov, I. Sergueev, Y.Z. Yue, B. Sepiol, P. Svec, L. Hu, R. Ruffer, Phys. Rev. B 82 (2010) 144301.
[22] L. Battezzati, A. Habib, D. Baldissin, P. Rizzi, J. Alloys Compd. 504S (2010) S48.
[23] X. Dong, J. Hu, Z. Huang, H. Wang, R. Gao, Z. Guo, Sci. Sintering 41 (2009) 199.
[24] D.M. Minić, A. Gavrilović, P. Angerer, D.G. Minić, A. Maričić, J. Alloys Compd. 482 (2009) 502.
[25] A. Kalezić-Glisović, L. Novaković, A. Maričić, D. Minić, N. Mitrović, Mater. Sci. Eng. B 131 (2006) 45.
[26] A. Maričić, M.M. Ristić, Sci. Sintering 35 (2003) 31.
[27] A.X.S. Bruker, TOPAS V3: General Profile and Structure Analysis Software for Powder Diffraction Data, Karlsruhe, 2005.
[28] G.K. Williamson, W. Hall, Acta Metall. 1 (1953) 22.
[29] D. Ritter, G. Ravichandran, 15th Technical Meeting DYMAT, Metz, 1–2 June, 2006.